

**The September 14, 2015 phreatomagmatic eruption of Nakadake first crater, Aso Volcano, Japan: Eruption sequence inferred from ballistic, pyroclastic density current and fallout deposits**

Yasuo Miyabuchi <sup>a,\*</sup>, Yoshiyuki Iizuka <sup>b</sup>, Chihoko Hara <sup>a,1</sup>, Akihiko Yokoo <sup>c</sup>,  
Takahiro Ohkura <sup>c</sup>

<sup>a</sup> Faculty of Education, Kumamoto University, Kurokami 2-40-1, Chuo-ku, Kumamoto 860-8555, Japan

<sup>b</sup> Institute of Earth Sciences, Academia Sinica, PO Box 1-55, Nankang, Taipei, Taiwan

<sup>c</sup> Aso Volcanological Laboratory, Institute for Geothermal Sciences, Graduate School of Science, Kyoto University, 3028 Sakanashi, Ichinomiya, Aso, Kumamoto 869-2611, Japan

\* Corresponding author

*E-mail address:* miyabuchi@gmail.com (Y. Miyabuchi)

TEL: +81-96-342-2545; FAX: +81-96-342-2545

<sup>1</sup> Present address: Nishikokubu Elementary School, 1972-1 Suwanomachi, Kurume, Fukuoka 830-0037, Japan

**Abstract**

An explosive eruption occurred at Nakadake first crater, Aso Volcano in central Kyushu, southwestern Japan, on September 14, 2015. The sequence and causes of the

eruption were reconstructed from the distribution, textures, grain-size, component and chemical characteristics of the related deposits, and video record. The eruptive deposits are divided into ballistics, pyroclastic density current and ash-fall deposits. A large number of ballistic clasts (mostly < 10 cm in diameter; maximum size 1.6 m) are scattered within about 500 m from the center of the crater. Almost half of the ballistics appear as fresh and unaltered basaltic andesite rocks interpreted to be derived from a fresh batch of magma, while the rest is weakly to highly altered clasts. A relatively thin ash derived from pyroclastic density currents covered an area of 2.3 km<sup>2</sup> with the SE-trending main axis and two minor axes to the NE and NW. The pyroclastic density current deposit (maximum thickness < 10 cm even at the crater rim) is wholly fine grained, containing no block-sized clasts. Based on the isopach map, the mass of the pyroclastic density current deposit was estimated at ca.  $5.2 \times 10^4$  tons. The ash-fall deposit is finer grained and clearly distributed to about 8 km west of the source crater. The mass of the ash-fall deposit was calculated at about  $2.7 \times 10^4$  tons. Adding the mass of the pyroclastic density current deposit, the total discharged mass of the September 14, 2015 eruption was  $7.9 \times 10^4$  tons. The September 14 pyroclastic density current and ash-fall deposits consist of glass shards (ca. 30%), crystals (20-30%) and lithic (40-50%) grains. Most glass shards are unaltered poorly crystallized pale brown glasses which probably resulted from quenching of juvenile magma. This suggests that the September 14, 2015 event at the Nakadake first crater was a phreatomagmatic eruption.

Similar phreatomagmatic eruptions occurred at the same crater on September 6, 1979 and April 20, 1990 whose eruptive masses were one order larger than that of the September 14, 2015 eruption. These events highlight the potential hazard from phreatic or phreatomagmatic eruptions at Nakadake first crater, and provide useful information that will assist in preventing or mitigating future disasters at other similar volcanoes worldwide.

*Keywords:* phreatomagmatic eruption; ballistic clasts; pyroclastic density current; Aso Volcano; Nakadake first crater

## 1. Introduction

Nakadake Volcano, which is the only active central cone inside the Aso caldera, is one of the most active volcanoes in Japan. The active crater (first crater) of Nakadake is occupied by a hot, hyperacidic ( $\text{pH} = 0.43$ ) crater lake during its calm periods (Miyabuchi and Terada, 2009; Ohsawa et al., 2010) and has maintained a high heat discharge rate of approximately 220 MW (Terada et al., 2008). During active periods, volcanic activity of Nakadake first crater is characterized by continuous fallout of black sandy ash from a dark eruption plume. The ash is interpreted to be derived from the solid glassy top of a magma column and is transported by a gas stream from below the solid top (Ono et al., 1995). In more active periods, strombolian eruptions have scattered red-hot scoriaceous clasts around the vent. Moreover, phreatic or phreatomagmatic eruptions occurred in June 1958, September 1979 and April 1990, ejecting coarse lithic blocks that are likely to cause human casualties near the crater and generating small low-temperature pyroclastic density currents (Taneda et al., 1959; Ono et al., 1982; Ikebe et al., 2008). These eruptions were relatively small in eruptive volume and magnitude, but they tend to impose a great hazard for areas within 1-2 km of the active crater, yet occasionally impossible to predict due to the lack of clear precursors.

In the last two decades, phreatic eruptions with accompanying ballistic projectiles occurred in other volcanoes such as Ruapehu (New Zealand) on September 25, 2007

(Christenson et al., 2010; Kilgour et al., 2010) and at Te Maari (New Zealand) on August 6, 2012 (Breard et al., 2014; Lube et al., 2014; Pardo et al., 2014). Moreover, a phreatic eruption at Ontake Volcano (central Japan) on September 27, 2014 caused 63 fatalities (including 5 missing persons) due to ballistic ejecta around the summit crater (Oikawa et al., 2015; Kaneko et al., 2016; Maeno et al., 2016), and the eruption resulted in the worst volcanic disaster in Japan during the past half-century. However, detailed geological and petrological studies on these eruptions and related deposits are poorly conducted, especially compared to strombolian, vulcanian and plinian eruptions.

We focus on the September 14, 2015 phreatomagmatic eruption at the Nakadake first crater, Aso Volcano. We describe the distribution, textures, grain-size, component and chemical characteristics of the associated deposits, and discuss the sequence and possible mechanism of the eruption in geological terms. This study provides further understanding of future explosive eruptions not only at Nakadake first crater but also at other similar volcanoes occupied by crater lakes.

## **2. Geological setting**

Aso Volcano is located in central Kyushu, southwestern Japan (Fig. 1A), and is one of the largest caldera volcanoes in the world. The caldera, 25 km north-south and 18 km east-west, was formed by four very large pyroclastic flow eruptions from ca. 270 ka to 90 ka (Ono et al., 1977; Matsumoto et al., 1991). Post-caldera cones (at least 17

cones), ranging from basalt to rhyolite, have arisen near the center of the caldera since the Aso-4 eruption at ca. 90 ka (Ono and Watanabe, 1985).

Nakadake Volcano is the only active central cone in Aso caldera, and is a composite volcano of basaltic andesite to basalt. Nakadake became active from ca. 22-21 ka (Miyabuchi et al., 2004), and has formed an old edifice (agglutinate and lava), a young edifice (pyroclasts and lava) and a still younger pyroclastic cone (Ono and Watanabe, 1985). The old volcanic edifice is the main cone of Nakadake Volcano, rising about 900 m from the caldera floor. The upper part of the edifice is a complex cone made largely of welded spatter, with subordinate amounts of other pyroclastic materials. The lower part of the edifice is composed mainly of lava flows. Recent tephrochronological studies (Miyabuchi et al., 2003, 2004; Miyabuchi, 2009) indicate that most of the edifice was constructed at ca. 22-21 ka. Thereafter, the western half of the upper edifice was destroyed by a northwestward-directed horseshoe-like collapse, leaving a 250-m-high collapsed crater wall (Ono et al., 1995). The young volcanic edifice is believed to have formed during Holocene time, and the youngest pyroclastic cone subsequently rose inside the young edifice (Ono and Watanabe, 1985). The active crater of Nakadake Volcano, formed in the youngest pyroclastic cone, is a composite of seven small craters aligned N-S (Fig. 1B). Only the northernmost crater (first crater) has been active in the past 80 years, although some others were active before the 1933 eruption (Fukuoka District Meteorological Observatory, 1965).

### **3. Outline of the September 14, 2015 eruption**

Following the 1988-1995 major activity including ash, strombolian and phreatomagmatic eruptions (Ikebe et al., 2008), surface unrest of the Nakadake first crater had mostly been mild, except for several small ash emissions through the hyperacid crater lake in 2003, 2004, 2005 and 2008 (Miyabuchi et al., 2008; Miyabuchi and Ikebe, 2008). The crater lake began to reduce in size from April 2013, and surface ratio of the lake water to the crater bottom became <10% after December 2013. Multiple small ash emissions occurred from the Nakadake first crater between January 13 and February 19, 2014 (Fukuoka District Meteorological Observatory, 2015a). Subsequently, the crater bottom dried up on July 12, and a vent near the center of the crater had been incandescent since July 28, 2014. A minor eruption was observed on August 30. Because of this eruption, Fukuoka District Meteorological Observatory (FDMO) of the Japan Meteorological Agency (JMA) made a Volcanic Warning (near-crater warning) changing the volcanic alert level from level 1 (normal condition) to level 2 (do not approach the crater) on the same day.

The Nakadake first crater began a series of magmatic eruptions on November 25, 2014. Relatively active eruptive events including gray ash plumes (<1500 m above the crater rim) and strombolian eruptions (<300 m) continued to May 3, 2015. These activities were restricted to the 141 vent, which was defined by JMA, formed near the

center of the Nakadake first crater. A pyroclastic cone was formed around the 141 vent by deposition of large amounts of ash and scoria (Yokoo and Miyabuchi, 2015). The southern half of the 141 pyroclastic cone disappeared probably due to a collapse accompanied by a felt earthquake on May 3 (Fukuoka District Meteorological Observatory, 2016). The total discharged mass of ash-fall deposits from November 2014 to May 2015 was estimated at  $2.1 \times 10^6$  tons. Thereafter, a small amount of hot water re-entered the 141 pyroclastic cone on June 10, and small eruptions occurred on August 8 and September 3. The maximum temperature of the water ranged from 80 to 90 °C, and several high-temperature areas of 100-400 °C were observed inside the 141 cone (Fukuoka District Meteorological Observatory, 2016). Crustal deformation related to inflation of magma reservoir was observed from July 2015.

On September 14, 2015, the Nakadake first crater erupted (Fig. 1C), generating impacts around the crater for the first time since September 1979. The amplitude of short period tremor began to gradually increase from the afternoon on September 10, and seismicity levels remained elevated (repeating fluctuation) until the September 14 eruption. Small eruptions on September 10-11 produced ash-fall deposits of ca. 1000 tons. We also observed intermittent, vigorous wet-ash emissions (<30 m high) inside the 141 cone on September 12. On September 14, another gradual increase of short-period tremor amplitude occurred at 09:18 (Japan Standard Time: JST; GMT + 9 h), and explosive activity started at 09:43 (Fukuoka District Meteorological Observatory,

2015b). Rising ash plumes, showers of ballistic ejecta and emergence of pyroclastic density currents (PDCs) during the eruption were recorded by a video camera operated by Nippon Hoso Kyokai (NHK; Japan Broadcasting Corporation) at about 1.1 km SW of the crater (location F in Fig. 1A). According to the video record, a gray to dark gray ash plume rose vertically from the crater rim around 09:44, although white plumes had been observed before the eruption. A dark gray to black vigorous plume was recognized at the east side of the first gray ash plume at 09:46:28. An ash column began to spill out of the crater and reached to the western slope at 09:47:04. Ballistic clasts falling on the northern to southwestern slopes were observed at 09:47:07-09:47:20. PDCs swept to the north at 09:47:14 and to the southwest at 09:47:16. A vigorous ash plume rose again at 09:47:22 and ballistic aprons were emplaced northwards at 09:47:25-09:47:38. A second series of PDCs travelled down to the west at 09:47:25 and to the south at 09:47:41, and the PDC activity completely stopped at 09:48:30. The maximum height of the ash plume was eyewitnessed at about 2000 m above the crater rim (Fukuoka District Meteorological Observatory, 2015b). The particulate fallout was dispersed to the west. Because of this eruption, FDMO made a Volcanic Warning changing the volcanic alert level from level 2 (do not approach the crater) to level 3 (do not approach the volcano).

After the September 14 eruption, intermittent small eruptions produced ash falls. On October 23, two explosive eruptions took place at 02:59 and 06:02 and their ash plumes rose 1400 m and 1600 m above the crater rim, respectively (Fukuoka District

Meteorological Observatory, 2016). Both eruptions accompanied ballistic fallout and severely damaged the crater rim area.

#### **4. Eruption deposits**

We performed fieldwork for observing and sampling of ash-fall deposits outside 1 km of the Nakadake first crater from 11:30 to 18:00 on September 14, 2015. A field visit to sample and measure the eruption deposits in the proximal area was carried out in the following morning under near-ideal atmospheric conditions, before significant modification by wind and rainwater by mixing with older deposits. However, limited time was spent in the crater area due to the risk of further eruptive activity. Based on these field observations, the eruption deposits were divided into three types; ballistics, pyroclastic density current deposit and ash-fall deposit.

##### *4.1. Ballistics*

The ballistic ejection during the September 14 eruption was recognized by the NHK video footage recorded at 1.1 km SW of the Nakadake first crater. Our fieldwork in the morning of September 15 confirmed that a large number of ballistic clasts were scattered from the southwestern rim of the Nakadake first crater to the southern rim of the second crater and that ballistics reached at least about 400 m south of the center of the first crater.

The spatial concentration of the ballistic deposits at the southern rim of Nakadake second crater (locality G in Fig. 1B) was relatively high ( $<100$  clasts/m<sup>2</sup>), and most clasts were a few centimeters in diameter (Fig. 2A). The maximum long-axis diameter is 35 cm at the southern rim. We observed that parts of wooden fences were destroyed by impacts of ballistics (Fig. 2B). In contrast, a lower concentration of ballistic clasts at the southwestern rim of Nakadake first crater (locality I) was observed (a few tens clasts/m<sup>2</sup>) than that at the southern rim of the second crater, but many large clasts of several ten centimeters in diameter could be recognized (Fig. 2C). The largest clast (1.6 × 1.0 × 0.7 m; Fig. 2D) was ejected to a distance of 230 m SW of the center of the first crater (locality K in Fig. 1B). Some ballistic clasts were covered by oxidized reddish ash. Several impact craters, which were  $< 1$  m in diameter, were observed on the surface of the southwestern crater rim.

We sampled all ballistic clasts from an area of 2.2 × 1.7 m (ca. 3.5 m<sup>2</sup>) on the roof top of a camera cabin of the Aso Volcano Museum located at the southwestern rim of Nakadake first crater (Fig. 3A; locality J in Fig. 1B). The total number of ballistic clasts deposited on the area was 158, corresponding to be 45 clasts/m<sup>2</sup> (equivalent to 4514 clasts/10×10 m). The ballistic clasts are dominated by basaltic andesite fragments of lavas or pyroclastic rocks. These are divided by varying degree of alteration into three types: fresh lithic, weakly altered lithic, and moderately to highly altered lithic (Fig. 3B). The fresh lithic clasts are separated into subangular to subrounded faceted lithic clasts

and bomb-shaped clasts. The bomb-shaped clasts are spherical to elongated in shape and some have cauliflower-shaped surface textures. These observations suggest that they deformed in a plastic manner during flight or after emplacement. Some weakly altered lithics appear to be fresh *prima facie*, but they have sublimates on the surfaces or vesicles. Most altered lithics originate from fragments of lavas or pyroclasts erupted during previous episodes of activity, and fragments of consolidated old ash (tuff) are included in the altered lithics because they are not apparently juvenile materials in the case of this eruption. The proportions of fresh, weakly altered and highly altered ballistic clasts are 53%, 27% and 20%, respectively.

We measured the size (lengths of long, median and short axis) and mass of all 158 sampled ballistic clasts (Fig. 4). The bulk density was determined by the glass bead method (Sasaki and Katsui, 1981). Although the size of the largest clast (fresh lithic) is  $31 \times 21 \times 14$  cm, the long axes of ballistic clasts are concentrated  $< 10$  cm (fresh lithic 86%, altered lithic 94-95%). The masses of most sampled clasts are  $< 0.5$  kg (maximum 3.1 kg). The bulk densities of fresh and altered lithic clasts range 920-2500 kg/m<sup>3</sup> and 810-3200 kg/m<sup>3</sup>, respectively. There is no significant differences in the size and mass between fresh and altered lithics, although altered lithics included a few dense clasts ( $>2500$  kg/m<sup>3</sup>).

A weighted ash sampler (bucket; 25 cm across and deep) was installed at the southwestern rim of the Nakadake first crater (locality J in Fig. 1B). The September 14

ash and several ballistic clasts were captured by the sampler. The upper side of the weight had no damage, while a part of the underside was melted (Fig. 5) by the heat of a clast (about 5 cm in diameter). Moreover, another clast adhered to the side face of the weight (Fig. 5B). The surface of the weight was covered with a sheet of low-density, cement-filled polyethylene. The melting points and ignition temperatures of these materials are 100-115 °C and about 350 °C, respectively. The surface of the weight was ignited by the clast, indicating that parts of ballistic clasts were over 350 °C during the eruption.

#### *4.2. Pyroclastic density current deposits*

Generation of at least two series of pyroclastic density currents (PDCs) was recorded by the NHK video camera, and photographed by many eye-witnesses (Fig. 1C). The PDC deposits were mapped by the Geological Survey of Japan (AIST), plotting the distribution of white ash on aerial photographs taken by JMA with Kyushu Regional Development Bureau (Ministry of Land, Infrastructure, Transport and Tourism) in the afternoon of September 14. The PDC deposits, which were seen as white to light-gray areas, were extent about 1.3 km southeast and 1.0 km northeast of the Nakadake first crater (Fig. 6; Fukuoka District Meteorological Observatory, 2015b). The JMA aerial inspection detected no notable high-temperature zone in the PDC deposits.

In addition to a field visit to the crater area in the morning on September 15, we

excavated many pits into the deposits in the proximal area to clarify the aerial extent and textures of PDC deposits, which were well preserved by the subsequent ash-fall deposits and the October 23 PDC deposits, from late October to late December 2015. These observations showed that an area of 2.3 km<sup>2</sup> was covered by a relatively thin ash interpreted to be derived from PDCs. The deposits were along a SE-trending main axis and two minor axes of the NE and NW (Fig. 1B). They ranged in thickness from 5 to 6 cm at the western to southwestern crater rims, and the maximum thickness of 8 cm was observed at the northwestern rim. Away from the crater rim, the deposits abruptly decreased in thickness to < 5 cm. Based on the isopach map (Fig. 1B), the volume of the PDC deposits is estimated at ca.  $6.8 \times 10^4$  m<sup>3</sup>: giving an erupted mass of ca.  $5.2 \times 10^4$  tons assuming a mean density of 1.3 g/cm<sup>3</sup> (our measured value).

At the southwestern rim of the Nakadake first crater, the September 14, 2015 eruption deposits were wholly fine grained beds containing no block-sized clasts, and could be divided into three units by grain-size and sorting characteristics as units 1 to 3 in ascending order (Fig. 7). Unit 1 is the first depositional unit that directly overlies the ~May 2015 ash-fall deposits. It is 1-2 cm thick at the SW crater rim and a gray, massive, matrix-supported, moderately sorted bed that consists mostly of medium- to coarse ash with ca. 5% lapilli. Above a gradational contact, unit 2 is a gray, massive, matrix-supported unit, and the thickness is 2 cm at the SW rim. It is slightly coarser grained and poorer sorted than unit 1, and is composed of coarse- to fine ash (75%) and

lapilli (13%). Unit 3 overlies a relatively sharp contact, and is a gray crudely-stratified, well-sorted bed. It is 2 cm thick and consists of fine to medium ash (67%) with silt to clay content of 21%. Unit 3 is finer grained and better sorted than the underlying units (units 1 and 2). The texture and grain-size characteristics of unit 3 suggest that the unit was deposited by ash-fall.

We installed three ash sampling buckets in the crater area (locations G, J, M in Fig. 1B), and they had been covered with polyethylene plastic bags before the September 14 eruption. At the southwestern crater rim, most of the plastic bag was lost, probably due to heat from ballistic clasts, but the bucket itself was not melted at all (Fig. 5A). At the southern rim of the second crater (ca. 370 m S of the center of first crater; locality G) and a site ca. 350 m SSW of the center of first crater (locality M), plastic bags covering ash samplers suffered with no damage. These observations suggest that the temperature of the PDCs was much lower than the melting point of polyethylene (100-115 °C).

#### *4.3. Ash-fall deposit*

We undertook fieldwork around the Nakadake crater from September 14 to 15, 2015, to examine the distribution and characteristics of the fallout tephra deposit associated with the September 14 eruption. Ash samples were obtained from the surfaces of man-made constructions including roads and concrete floors at distal 44 sites (>1 km of crater) and above previous eruption deposits at proximal 5 sites (SW

crater rim). The samples were dried and their masses were measured. By plotting their values on the distribution map, nine isopleths (7000, 5000, 2000, 1000, 500, 200, 100, 50, 20 g/m<sup>2</sup>) were delineated (Fig. 1A).

The ash-fall deposit was distributed about 8 km to the west of the source crater. The dispersal axis extends about 4 km to the northwest, then changes to west-southwest (Fig. 1A). The ash distribution is consistent with the wind direction of east-northeast (ca. 5 m/s, 1500 m asl at 09:50) analyzed by JMA. We observed the ash fall at Ozu town about 20 km west of the crater at 10:30 on September 14. Moreover, the ash fall was recognized in the southern part of Fukuoka prefecture (~60 km NW of crater; Fukuoka District Meteorological Observatory, 2015b).

The ash-fall deposit is gray in color (N5/0; Munsell color) and contains small amounts of white lithic fragments (< 1 mm in diameter; Fig. 8A). At distal sites > 1.7 km from the vent, the fallout ash is composed mainly of sand-size particles with silt to clay content of about 20% but is partially aggregated at sizes of a few mm to 1 cm (Fig. 8B). The aggregated muddy ash of < 1 cm in diameter adhered on the crater-facing surface of a building located at 1.7 km northwest of the vent.

We calculated the mass of the September 14 ash-fall deposit using the relation between the area enclosed by each isopleth and the mass. In the proximal area where the ash deposited was > 7 kg/m<sup>2</sup>, we extrapolated the straight line that connects 5 kg/m<sup>2</sup> with 7 kg/m<sup>2</sup> to the area of the source vent (ca. 20 m in diameter). No such mass

calculation was performed in distal areas where the ash deposited was  $< 20 \text{ g/m}^2$ . We divided the relation between mass and area into nine sections, and the amount of mass in each section was calculated by integration. This method indicates that the mass of the ash-fall deposit was about  $2.7 \times 10^4$  tons. Adding the mass of the PDC deposits ( $5.2 \times 10^4$  tons), the total discharged mass of the September 14 eruption was  $7.9 \times 10^4$  tons.

## 5. Grain-size characteristic of deposits

The September 14, 2015 eruption deposits were mechanically sieved for grain-size analysis. The samples were dried and sieved at  $1 \phi$  intervals from  $-5$  to  $5 \phi$  ( $32\text{-}1/32$  mm). The median diameters ( $Md_\phi$ ), the Inman (1952) sorting coefficients ( $\sigma_\phi$ ) and skewness ( $\alpha_\phi$ ), and the Walker (1983) parameters of F1 (weight percentage finer than 1 mm) and F2 (weight percentage finer than  $1/16$  mm) were calculated.

The grain-size distributions for the PDC deposits are clearly unimodal (Fig. 9A). The unit 1 and unit 2 deposits show peaks at  $0$  to  $2 \phi$  and  $1$  to  $2 \phi$ , respectively. Unit 2 is poorer sorted than unit 1 at a site  $0.2$  km SW of the center of Nakadake first crater (locality J), but at  $0.3$  km SW (locality L) the two units display similar sorting. The grain-size distributions of the ash-fall deposits are predominantly unimodal, having peaks at  $2$  to  $5 \phi$  and are better sorted than the PDC deposits (Fig. 9A). Distal samples of the ash-fall deposits ( $>2$  km) reveal better sorting than proximal samples. Some ash-fall samples have skewed distributions on either side of the peaks.

Grain-size plots for the September 14 PDC deposits on a  $Md_{\phi}$  and  $\sigma_{\phi}$  diagram (Walker, 1971) show that they are moderately sorted ( $\sigma_{\phi}$ , 1.61 to 2.16, average 1.78) and fall within the pyroclastic surge field rather than the pyroclastic flow field of Walker (1971, 1983). The September 14 PDC deposits are much finer grained and better sorted than the Nakadake 19 ka bomb-and-ash flow deposit (Miyabuchi et al., 2006) and the Unzen 1991-1995 block-and-ash flow deposits (Miyabuchi, 1999), and are similar to the 1991-1995 Unzen ash-cloud surge deposits (Fig. 10A). The September 14 ash-fall deposits are finer and better sorted ( $\sigma_{\phi}$ , 1.09 to 1.69, average 1.41) than the PDC deposits. On plots of F2 versus F1 (Fig. 10B), the September 14 PDC deposits lie lower than the pyroclastic surge field of Walker (1983). Although they have relatively high F1 values, they display low F2 values, indicating their fines-depleted nature. The results of grain-size analysis suggest that the September 14, 2015 PDCs at Nakadake first crater were closer to pyroclastic surges rather than pyroclastic flows.

## **6. Component characteristic of the deposits**

Typical samples of the September 14 deposits were examined under a polarizing microscope in order to clarify their components. The samples were washed ultrasonically for ca. 10 min and dry sieved. Ash grains in the fraction of 3-2  $\phi$  (0.125-0.25 mm) were set in an epoxy resin to be fixed to slide glasses. Double-polished thin sections of the samples were then prepared for examination. The polarizing

microscope observations reveal that all samples of the September 14 deposits consist of glass shards, crystal and lithic grains. The glass particles are divided by color into transparent, pale brown, brown and black glasses (Fig. 9B). They are also separated by their shapes into block and scoria type particles (Fig. 9C). The crystals are single phenocrysts of plagioclase, olivine and clinopyroxene. Some phenocrysts have adhering different phenocrysts and/or glassy fragments. Lithic fragments are divided by color into black, brown, pale brown and translucent grains. The proportions of these components were determined by counting at least 200 grains in each thin section. The components of the September 6, 1979 and April 20, 1990 ash, which are products of phreatic or phreatomagmatic eruptions at same crater (Ono et al., 1982; Ikebe et al., 2008), were also examined for comparison.

Lithic fragments are abundant in both the PDC and ash-fall deposits, and the proportions range from 37 to 60% (Fig. 9B). They are moderately to highly crystallized and show varying degrees of alteration. Therefore, they are interpreted to be derived from lavas or pyroclastics of previous eruptions. The proportion of glass shards in the September 14 deposits is 22-28%. Pale brown glass shards are dominant (14-21%), but brown (2-5%) and black (1-2%) glasses are also observed. Poorly to moderately vesiculated blocky glass shards are dominant in the glass fraction (Fig. 9C) although a small amount of scoria type glasses (2%) is contained in the lower part of the PDC deposit (unit 1). Most glass shards appear as fresh and unaltered under polarizing

microscope observation (Fig. 11A). Proportions of glass shards of the September 14 deposits are slightly smaller than that of the April 1990 ash (39%) and larger than that of the September 1979 ash (16%).

Fractions coarser than 2  $\phi$  (0.25 mm) of only four samples (two PDC and two fall deposits) of the September 14 deposits were examined under a binocular microscope. Components of fractions coarser than 2 to -1  $\phi$  (0.25-2 mm) are almost identical to that of 3-2  $\phi$  although fractions coarser than -1  $\phi$  are composed only of lithic fragments (Fig. 9A). Most of the lithic fragments are dark gray to black in color.

Detailed textural observation of glass shards included in the September 14 ash-fall and PDC deposits was made using a scanning electron microscope (SEM; Hitachi TM-1000). As mentioned above, most of the glass shards are characterized by typical blocky textures (Fig. 12). The blocky glass shards are angular to subangular, and moderately vesiculated. Their shapes are dominated by curvilinear breakage surfaces. Most glass shards have adhering materials (e.g. gypsum) on their surfaces, especially in vesicle hollows.

Thin sections of representative samples of fresh, weakly altered and highly altered ballistic clasts were also examined under a polarizing microscope. The fresh clasts appear to be fusions of brown to black unaltered glasses with small amounts of phenocrysts (Fig. 11B). Rare sublimates are observed in the vesicles. In contrast, the textures of altered clasts are quite different from that of fresh lithic clasts. The weakly

altered clasts include plagioclase, clinopyroxene and olivine phenocrysts and have hyalopilitic to hyalo-ophitic groundmass textures. The vesicles are filled with various sublimates (Fig. 11C). The highly altered clast is porphyritic with large amounts of plagioclase, clinopyroxene, olivine phenocrysts and displays intersertal groundmass texture (Fig. 11D).

## **7. Chemical compositions of deposits**

### *7.1. Glass shard chemistry*

Major element chemical compositions of volcanic glass shards have been studied for the September 14 PDC and ash-fall deposits, and ash-fall deposits from May 2015, November 2014, April 20, 1990 and September 6, 1979 eruptions at the Institute of Earth Sciences, Academia Sinica, Taipei. Ash samples were mounted with epoxy resin. The mounted specimens were grounded with SiC (silicon carbide) papers from grid #400 to #2000 until a flat surface was exposed, then polished with 3  $\mu\text{m}$  and 1  $\mu\text{m}$  aluminum particulate compounds on rotation disks. The final polish was made by a vibration polisher (Buhler: Vibromet-2) with 0.3  $\mu\text{m}$  alumina compounds for several hours. The polished specimens were then coated with a layer of carbon (Q150TE, Quorum Technologies Ltd., UK) to facilitate electron conductance. First we investigated the polished samples employing petrographic and binocular microscopes, and examined shape and colors. The micro-textures and chemistries of glasses and minerals were

studied qualitatively using a field emission scanning electron microscope (FE-SEM: JEOL JSM-7100F); identification of minerals was made by an energy-dispersive spectrometer (EDS: Oxford Instruments Ltd., INCA-350) equipped with an FE-SEM, under beam conditions of 15 kV, and 0.1 nA acceleration voltage, and current, respectively. Chemical compositions of glass shards were determined by electron probe micro analyzers (JEOL EPMA JXA-8500F) equipped with five wave-length dispersive spectrometers (WDS). Secondary- and back-scattered electron images were used to guide the analysis on target positions of minerals. A 2  $\mu\text{m}$  defocused beam was operated for quantitative analysis at an acceleration voltage of 12 kV with a beam current of 6 nA. Measured X-ray intensities were ZAF-corrected using the standard calibration of synthetic (s) and natural (n) standard minerals with various diffracting crystals, as follows: wollastonite (s) for Si with TAP crystal, rutile (s) for Ti with PET crystal, corundum (s) for Al (TAP), chromium oxide (s) for Cr (PET), hematite (n) for Fe with LiF crystal, tephroite (s) for Mn (PET), periclase (s) for Mg (TAP), wollastonite (s) for Ca (PET), albite (n) for Na (TAP), and adularia (n) for K (PET). Counting times were 10 s for peak and 5 s for each upper and lower baselines of all elements. Standards run as unknowns yielded major oxide relative standard deviations for Si, Na and K of < 1%, and < 0.5% for other elements. Detection limits, based on 3  $\sigma$  of standard calibration, were < 600 ppm for all elements.

The mean values and standard deviations of major chemical compositions of

volcanic glass shards in each sample are shown in Table 1. On the FeO\*, CaO, Na<sub>2</sub>O and K<sub>2</sub>O versus SiO<sub>2</sub> diagrams (Fig. 13), the plots of glass shards included in the September 14 deposits overlap with those of glasses from the May 2015, November 2014, April 20, 1990 and September 6, 1979 eruptions. In September 14, 2015 deposits, black to brown glass shards tend to have relatively wider ranges of Al<sub>2</sub>O<sub>3</sub>, FeO\*, MgO, CaO, Na<sub>2</sub>O and K<sub>2</sub>O contents than those of pale brown glasses (Table 1).

Back-scattered electron (BSE) images of representative glass shards included in the September 14 deposits are shown in Fig. 14. No microlites are present in most of pale brown glasses (Fig. 14B), whereas black glass shards include titano-magnetite (higher contrast grains), clinopyroxene (intermediate) and plagioclase (darker) as microlites (Figs. 14C, D). Although these grain sizes are too small to be analyzed quantitatively, they are qualitatively identified by FE-SEM with EDS. Furthermore, some dark color glass shards contain numerous nanometer-scale crystals (nanolites; Sharp et al., 1996). Both microlites (>1 μm) and nanolites are recognized in some dark color glass grains (Fig. 14F). These nanolites are mostly Ca-rich plagioclase (darker color crystals; Figs. 14E and F) and Fe-oxides (higher contrast crystals; Fig. 14F) which were confirmed by FE-SEM with EDS as well. Dendrite textures of Ca-rich plagioclase microlites and nanolites are observed in some glass shards by BSE images.

## *7.2. Hydrothermal altered minerals*

X-ray powder diffraction (XRD) analysis was performed to identify fine hydrothermally altered minerals included in the September 14, 2015, April 20, 1990, and September 6, 1979, deposits. Fine fractions (finer than 8  $\phi$ ) of these ash samples were separated by the gravitational precipitation method, and then used for XRD analysis. The analysis was carried out with Rigaku MultiFlex X-ray diffractometer at the Center of Advanced Instrumental Analysis, Kyushu University. Measurements were performed at a scan speed of 1° per min from 3° to 60° using a CuK $\alpha$  target X-ray tube with an acceleration voltage of 40 kV and a filament current of 30 mA.

The XRD measurement showed that alunite, quartz, zeolite and montmorillonite occur in the September 14, 2015 deposit (Fig. 15). The April 20, 1990 and September 6, 1979 deposits contain alunite, jarosite, quartz and zeolite.

## **8. Discussion**

### *8.1. Origin of unaltered glass shards and fresh ballistic clasts*

Deposits of the September 14, 2015, eruption from the Nakadake first crater are characterized by 22-28% of glass shards and 53% of fresh ballistic clasts although they contain abundant altered lithic fragments. It is very important to determine whether these glass shards and fresh clasts are juvenile materials originating from newly ascending magma in order to understand the eruptive mechanism. The chemical

compositions of glass shards included in the September 14 deposits are similar to November 2014-May 2015, April 1990 and September 1979 ash from the Nakadake first crater (Fig. 13). It is therefore difficult to determine whether the glass shards are juvenile based only on the chemical compositions. These glass shards are fresh and unaltered under the polarizing microscope. SEM analysis also confirms that fresh glass shards have a blocky texture and lustrous surfaces with rounded vesicles although most glass shards have adhering materials on their surfaces (Fig. 12).

These glass shards and fresh ballistic clasts may have been produced during the previous period of activity (November 2014-May 2015) and stored on the crater bottom and/or inside the active vent and conduit until they were ejected on September 14, 2015. However, a hyperacid hot water existed in the center of the crater after June 2015 and the crater bottom was strongly affected by volcanic gas. Geshi and Shinohara (2012) experimentally confirmed that dissolved textures including etching pits were formed on the surfaces of glass particles in a man-made hyperacid water with composition was similar to that of Nakadake crater-lake water within a few minutes to a few hours. It is unlikely that erupted materials from the November 2014-May 2015 events remained without alteration under the hyperacid environment. More than half of the September 14 deposits are weakly to highly altered ash and clasts. We therefore propose that the unaltered glass shards and fresh ballistic clasts, which are contained in the September 14 deposits, are juvenile materials originating from molten to semi-solidified parts of

newly ascending magma (Fig. 16). The difference in color of glass shards reflects varying degrees of crystallinity in glass particles. Black glasses, which are highly crystallized (Figs. 14A, C and D), are likely to derive from a slow cooling outer or upper part of conduit. In contrast, pale brown glasses, which contain only rare microlites (Figs. 14A, B), appear to have come from a molten inner part of conduit and resulted from rapid cooling because they are poorly crystallized. Fresh ballistic clasts, which are composed of unaltered black to brown glasses (Figs. 11B), are likely to derive from a semi-solidified part of conduit. As mentioned before, black to brown glass shards tend to have relatively wider ranges of FeO\*, CaO, Na<sub>2</sub>O and K<sub>2</sub>O contents than those of pale brown glasses (Fig. 13). This fact probably reflects that black to brown glasses contain both microlites and nanolites (Figs. 14E and F). In contrast, because pale brown glasses include rare microlites and nanolites, the chemical composition is concentrated in a narrow range.

Here we examine examples describing deposits associated with phreatic eruptions at other volcanoes to compare with the September 14, 2015 Nakadake eruption. The September 27, 2014 eruption at Ontake Volcano produced numerous ballistic ejecta (Tsunematsu et al., 2016), proximal PDC and fallout deposits (Maeno et al., 2016). Since no fresh juvenile components could be found in the deposits, the eruption was interpreted to be a phreatic eruption despite its larger deposit volume than the September 14, 2015 Nakadake eruption. The August 6, 2012 eruption of Upper Te

Maari Crater in New Zealand produced violent PDCs and numerous ballistic blocks (Breard et al., 2014; Lube et al., 2014; Pardo et al., 2014). It is described as a hydrothermal eruption because the deposits were composed mostly of blocks of lava and scoria that had erupted during previous volcanic episodes, a variety of crater-floor sediments and vent-fill debris.

In contrast, the September 25, 2007 eruption at Ruapehu Crater Lake generated a directed ballistic fallout apron and surtseyan jet (Kilgour et al., 2010), and the deposits contained up to 5% of fresh glasses, which were thought to be juvenile materials (Christenson et al., 2010). The August 2014 and May 2015 eruptions of Kuchinoerabujima Volcano (SW Japan) produced ballistic blocks and PDCs, and the eruptive deposits included small amounts of non-altered glassy grains (~10%), which were likely to be juvenile materials (Geshi et al., 2016). Also in the case of September 14, 2015 Nakadake eruption, the deposits contain 20-50% of fresh and unaltered materials interpreted to be derived from a newly ascending magma. The higher proportion of juvenile materials therefore suggests that the September 14, 2015 Nakadake eruption is a phreatomagmatic eruption although the eruption is one or two orders of magnitude smaller in eruptive volume than recent examples in these Japanese and New Zealand volcanoes.

## 8.2. Eruption sequence

The sequence and causes of the September 14, 2015 phreatomagmatic eruption at Nakadake first crater can be reconstructed from the distribution and characteristics of eruptive deposits and video record (Fig. 16). Following the November 2014-May 2015 magmatic activity including ash and strombolian eruptions, surface unrest at Nakadake first crater was mostly mild, and hyperacid hot water reformed in the crater after June 2015. The existence of ground water during calm and active periods was confirmed near the level of the bottom of Nakadake first crater by annual temperature variation in bore holes near the crater (Sudo and Hurst, 1998). We believe that decrease in temperature around the Nakadake first crater favored the return of an aquifer near the conduit under the vent. However, small amount of magma remained at shallow levels, and small eruptions occurred on August 8 and September 3 (Fukuoka District Meteorological Observatory, 2015b, 2016). The gradual increase of short-period tremor amplitude from the afternoon on September 10 suggests the ascent of magma body related to the September 14 eruption, and caused small ash emissions of 1000 tons on September 10-11 and intermittent vigorous wet ash emissions inside the crater on September 12 (Fig. 16A).

The proximate cause of the September 14, 2015 eruption was that the magma came in contact directly with an aquifer. The contact of magma and water might have occurred from 09:18 when the amplitude of short-period tremor increased (Fig. 16B).

This led to a rapid pressure increase of inside the conduit under the vent, and resulted in the first gray to dark gray ash plume rising vertically from the Nakadake first crater. The remarkable increase of tremor amplitude suggests that the September 14 eruption began at 09:43. The rapid release of gas and ash led to the opening of a vent buried by crater-floor sediments and surficial hot water, and propagated depressurization downward (Fig. 16C). The resulting combined burst of gas and entrained particulate materials broke the semi-solidified magma head, which included highly crystallized black glasses, hydrothermally altered rocks (lavas and agglutinates) and tephra surrounding the conduit (Fig. 16D), generating ballistic ejecta apron, a cock's tail jet and high steam column at 09:47:07-09:47:20 (time from the NHK video record). Subsequently, smaller (a few hundred meter high) gray to dark gray columns spilled out of the Nakadake first crater, resulting in generation of pyroclastic density currents (PDCs) at 09:47:14-09:47:16 (Fig. 16E). The PDCs did not appear to be column-collapse type PDCs from the video record, and were dilute and low-temperature currents mostly comprising sand- and silt-sized particles. They were thinly spread over < 1-1.3 km from the vent and were not thick even at the crater rim. According to the NHK video footage, ballistic clasts were thrown again to the north at 09:47:25-09:47:38 immediately after a vigorous dark gray ash plume (09:47:22) and second PDCs swept down to the west at 09:47:25 and to the south at 09:47:41. PDCs cascading to all directions completely stopped at 09:48:30. Ash fall was clearly observed within 8 km to

the west of the source crater, but the tephra dispersal was reported to extend to ~60 km from the vent. The ash-fall deposit is thought to have developed from direct rising plume and co-PDC plumes (Fig. 16E).

At least two PDC events were preceded by ballistic ejecta respectively. Almost half of ballistic clasts likely originated from a semi-solidified part of magma head (rich in highly crystallized black glasses) and had temperatures of  $> 350$  °C during the eruption although temperatures of PDCs were much lower than 100-115 °C. Release of numerous ballistic ejecta comprising both the magma head and previous erupted materials led to a vent enlargement, resulting in explosive ejection of gas and ash, finally forming vertically rising plumes and PDCs. A large amount of water was thought to exist around the conduit before the eruption. Therefore, the ascending plumes remained cold and rapidly became denser than the atmosphere. The ash aggregation observed in the fallout deposit (Fig. 8B) also indicates that the rising plume contained a small amount of water. Consequently, fountain collapse may have occurred, and the relatively low-temperature PDCs spread out from the crater.

### *8.3. Implications for hazard assessment*

The September 14, 2015 phreatomagmatic eruption of the Nakadake first crater occurred late in the 2014-2015 eruptive activity and generated a ballistic ejecta apron, pyroclastic density currents and leeward-dispersed ash-fall. Previous phreatomagmatic

or phreatic eruptions including the September 6, 1979 and April 20, 1990 events at the same crater also took place in the late stages of the active periods (Ikebe et al., 2008). In all these eruptions, the crater lake or hot water inside the crater was restored in the late stage of the active period. This fact suggests that the crater lake re-forming may correspond to the occurrence of explosive eruptions rather than the most active period characterized by ash and strombolian eruptions in the case of Nakadake first crater.

Phreatic or phreatomagmatic eruptions occasionally occur without clear precursor signals. In the case of the September 14, 2015 Nakadake eruption, the amplitude of short-period tremor began to increase four days prior to the eruption, and then seismicity levels remained elevated until the eruption. Moreover, another gradual increase of amplitude of short-period tremors, which probably indicates magma and water interactions, was observed ca. 25 min before the onset of eruption. These seismic records are thought to be precursor phenomena of the September 14 eruption. Therefore, seismic monitoring is very important for predicting these phreatic or phreatomagmatic eruptions at the Nakadake first crater.

## **9. Conclusions**

Following the November 2014-May 2015 magmatic activity, an explosive eruption occurred at Nakadake first crater, Aso Volcano, on September 14, 2015. The deposits of this event provided an opportunity to understand processes involved in an explosive

eruption at a crater-lake volcano. The September 14 eruption was caused by the contact of magma directly with an aquifer. The resulting combined burst of gas and entrained particulate materials broke the semi-solidified magma head, hydrothermally altered materials surrounding the conduit, consequently generating ballistic ejecta apron and pyroclastic density currents around the crater. The eruptive products are characterized by the existences of unaltered glass shards (~30%) and fresh ballistic clasts (ca. 50%), which are interpreted to be juvenile materials originating from molten to semi-solidified parts of newly ascending magma.

Phreatic or phreatomagmatic eruptions frequently occur at crater-lake volcanoes worldwide. This type of eruption is potentially energetic and hazardous for areas within a few km of the active crater. Although seismic observations are mostly performed, these eruptions occasionally occur without detecting clear precursor signals. However, there are several examples that inflation of volcanic edifices and/or activation of fumarolic activity were recognized as precursory phenomena (e.g., Geshi et al., 2016). Also in the case of the September 14, 2015 Nakadake eruption, we could confirm gradual increase of short-period tremor amplitude four days prior to the eruption. Careful geophysical and visual observations are needed to predict future phreatic or phreatomagmatic eruptions. Furthermore, the identification of juvenile materials and examination of their petrological characteristics are fundamental to understand the sequence and mechanism of these eruptions. However, insightful petrological

examinations of deposits from phreatic or phreatomagmatic eruptions have been poorly performed. This study can be used to provide information for estimating future phreatomagmatic eruptions not only at Nakadake first crater but also at other similar volcanoes occupied by crater lakes.

### **Acknowledgements**

Parts of fieldwork were undertaken with Hideho Inoue, Shin-ichi Matsusue and Mitsuru Utsugi. Video record provided by the NHK Kumamoto Broadcasting station was very useful to understand the detailed sequence of the September 14, 2015 Nakadake eruption. The Aso Summit Office (Aso City) gave us permission for our field survey. The XRD analysis was performed by Midori Watanabe and sample preparation for the analysis was supported by Takashi Kusaba and Noriko Yamaguchi. We thank Kenji Shida for the identification of altered minerals. The eruption photograph and aerial photograph were provided by Yuka Matsushima and the Japan Meteorological Agency (Fukuoka District Meteorological Observatory), respectively. Discussions with Nobuo Geshi and Hideo Hoshizumi concerning deposits and activity of Nakadake first crater were very helpful. The paper was improved by constructive comments from Nancy Riggs and an anonymous reviewer. This study was supported by the Ministry of Education, Culture, Sports, Science and Technology (MEXT) of Japan, under its Earthquake and Volcano Hazards Observation and Research Program (No. 1802).

## References

- Breard, E.C.P., Lube, G., Cronin, S.J., Fitzgerald, R., Kennedy, B., Scheu, B., Montanaro, C., White, J.D.L., Tost, M., Procter, J.N., Moebis, A., 2014. Using the Spatial distribution and lithology of ballistic blocks to interpret eruption sequence and dynamics: August 6 2012 Upper Te Maari eruption, New Zealand. *J. Volcanol. Geotherm. Res.* 286, 373-386.
- Christenson, B.W., Reyes, A.G., Young, R., Moebis, A., Sherburn, S., Cole-Baker, J., Britten, K., 2010. Cyclic processes and factors leading to phreatic eruption events: Insights from the 25 September 2007 eruption through Ruapehu Crater Lake, New Zealand. *J. Volcanol. Geotherm. Res.* 191, 15-32.
- Fukuoka District Meteorological Observatory, 1965. Eruptive history of Aso Volcano. *Memoirs of Fukuoka District Meteorological Observatory* 20, 15-46 (in Japanese).
- Fukuoka District Meteorological Observatory, 2015a. Volcanic Regular Bulletin of Aso Volcano in 2014. 21p (in Japanese).
- Fukuoka District Meteorological Observatory, 2015b. Volcanic Regular Bulletin of Aso Volcano in September 2015. 15p (in Japanese).
- Fukuoka District Meteorological Observatory, 2016. Volcanic Regular Bulletin of Aso Volcano in 2015. 31p (in Japanese).
- Geshi, N., Shinohara, H., 2012. Shallow conduit process of Aso volcano inferred from the ejecta in May 2011. *Chikyū Monthly* 34, 679-684 (in Japanese).

- Geshi, N., Iguchi, M., Shinohara, H., 2016. Phreatomagmatic eruptions of 2014 and 2015 in Kuchinoerabujima Volcano triggered by a shallow intrusion of magma. *J. Nat. Dis. Sci.* 37, 67-78.
- Ikebe, S., Watanabe, K., Miyabuchi, Y., 2008. The sequence and style of the 1988-1995 eruptions of Nakadake, Aso Volcano, Kyushu, Japan. *Bull. Volcanol. Soc. Japan* 53, 15-33 (in Japanese with English abstract).
- Inman, D.L., 1952. Measures of describing the size distribution of sediments. *J. Sediment. Petrol.* 22, 125-145.
- Kaneko, T., Maeno, F., Nakada, S., 2016. 2014 Mount Ontake eruption: characteristics of the phreatic eruption as inferred from aerial observations. *Earth Planets Space* 68, 72.
- Kilgour, G., Manville, V., Della Pasqua, F., Graettinger, A., Hodgson, K.A., Jolly, G.E., 2010. The 25 September 2007 eruption of Mount Ruapehu, New Zealand: directed ballistics, Surtseyan jets, and ice-slurry lahars. *J. Volcanol. Geotherm. Res.* 191, 1-14.
- Lube, G., Breard, E.C.P., Cronin, S.J., Procter, J.N., Brenna, M., Moebis, A., Pardo, N., Stewart, R.B., Jolly, A., Fournier, N., 2014. Dynamics of surges generated by hydrothermal blasts during the 6 August 2012 Te Maari eruption, Mt. Tongariro, New Zealand. *J. Volcanol. Geotherm. Res.* 286, 348–366.
- Maeno, F., Nakada, S., Oikawa, T., Yoshimoto, M., Komori, J., Ishizuka, Y., Takeshita,

- Y., Shimano, T., Kaneko, T., Nagai, M., 2016. Reconstruction of a phreatic eruption on 27 September 2014 at Ontake volcano, central Japan, based on proximal pyroclastic density current and fallout deposits. *Earth Planets Space* 68, 82.
- Matsumoto, A., Uto, K., Ono, K., Watanabe, K., 1991. K-Ar age determinations for Aso volcanic rocks: concordance with volcanostratigraphy and application to pyroclastic flows. *Programme and Abstracts of the Volcanological Society of Japan 1991(2)*, 73 (in Japanese).
- Miyabuchi, Y., 1999. Deposits associated with the 1990-1995 eruption of Unzen volcano, Japan. *J. Volcanol. Geotherm. Res.* 89, 139-158.
- Miyabuchi, Y., 2009. A 90,000-year tephrostratigraphic framework of Aso Volcano, Japan. *Sediment, Geol.* 220, 169-189.
- Miyabuchi, Y., Ikebe, S., 2008. The February 2008 ash deposit from the Nakadake crater, Aso Volcano, Japan. *Bull. Volcanol. Soc. Japan* 53, 201-206 (in Japanese with English abstract).
- Miyabuchi, Y., Terada, A., 2009. Subaqueous geothermal activity revealed by lacustrine sediments of the acidic Nakadake crater lake, Aso Volcano, Japan. *J. Volcanol. Geotherm. Res.* 187, 140-145.
- Miyabuchi, Y., Hoshizumi, H., Takada, H., Watanabe, K., Xu, S., 2003. Pumice-fall deposits from Aso volcano during the past 90,000 years, southwestern Japan. *Bull. Volcanol. Soc. Japan* 48, 195-214 (in Japanese with English abstract).

- Miyabuchi, Y., Hoshizumi, H., Watanabe, K., 2004. Late-Pleistocene tephrostratigraphy of Aso Volcano, southwestern Japan, after deposition of AT ash. *Bull. Volcanol. Soc. Japan* 49, 51-64 (in Japanese with English abstract).
- Miyabuchi, Y., Watanabe, K., Egawa, Y., 2006. Bomb-rich basaltic pyroclastic flow deposit from Nakadake, Aso Volcano, southwestern Japan. *J. Volcanol. Geotherm. Res.* 155, 90-103.
- Miyabuchi, Y., Ikebe, S., Watanabe, K., 2008. Geological constraints on the 2003-2005 ash emissions from the Nakadake crater lake, Aso Volcano, Japan. *J. Volcanol. Geotherm. Res.* 178, 169-183.
- Ohsawa, S., Saito, T., Yoshikawa, S., Mawatari, H., Yamada, M., Amita, K., Takamatsu, N., Sudo, Y., Kagiya, T., 2010. Color change of lake water at the active crater lake of Aso volcano, Yudamari, Japan: is it in response to change in water quality induced by volcanic activity? *Limnology* 11, 207-215.
- Oikawa, T., Yamaoka, K., Yoshimoto, M., Nakada, S., Takeshita, Y., Maeno, F., Ishizuka, Y., Komori, J., Shimano, T., Nakano, S., 2015. The 2014 eruption of Ontake Volcano, central Japan. *Bull. Volcanol. Soc. Japan* 60, 411-415 (in Japanese).
- Ono, K., Watanabe, K., 1985. Geological map of Aso Volcano 1:50,000. *Geological Map of Volcanoes 4*, Geological Survey of Japan (in Japanese with English abstract).
- Ono, K., Matsumoto, Y., Miyahisa, M., Teraoka, Y., Kambe, N., 1977. Geology of the Taketa district. Geological Survey of Japan, 145p (in Japanese with English

abstract).

Ono, K., Shimokawa, K., Soya, T., Watanabe, K., 1982. Geological and petrological study on the ejecta of 1979 eruption of Nakadake, Aso volcano, Japan. Report on an urgent study of 1979 eruption of Ontake and Aso volcano, Science and Technology Agency, 167-189 (in Japanese).

Ono, K., Watanabe, K., Hoshizumi, H., Ikebe, S., 1995. Ash eruption of the Naka-dake crater, Aso volcano, southwestern Japan. *J. Volcanol. Geotherm. Res.* 66, 137-148.

Pardo, N., Cronin, S.J., Nemeth, K., Brenna, M., Schipper, C.I., Breard, E., White, J.D.L., Procter, J., Stewart, B., Agustín-Flores, J., Zernack, A., Kereszturi, G., Lube, G., Auer, A., Neall, V., Wallace, C., 2014. Perils in distinguishing phreatic from phreatomagmatic ash; insights into the eruption mechanisms of the 6 August 2012 Mt. Tongariro eruption, New Zealand. *J. Volcanol. Geotherm. Res.* 286, 397–414.

Sasaki, T., Katsui, Y., 1981. Density of pumice using glass beads. *Bull. Volcanol. Soc. Japan* 26, 117–118 (in Japanese).

Sharp, T.G., Stevenson, R.J., Dingwell, D.B., 1996. Microlites and “nanolites” in rhyolitic glass: microstructural and chemical characterization. *Bull. Volcanol.* 57, 631-640.

Sudo, Y., Hurst, A.W., 1998. Temperature changes at depths to 150 metres near the active crater of Aso Volcano: preliminary analysis of seasonal and volcanic effects. *J. Volcanol. Geotherm. Res.* 81, 159-172.

- Taneda, S., Matsumoto, Y., Miyachi, S., Miyachi, M., Ishibashi, K., Kojima, M., 1959. The 1958 June eruption of Volcano Aso. *Bull. Volcanol. Soc. Japan* 3, 136–146 (in Japanese with English abstract).
- Terada, A., Hashimoto, T., Kagiya, T., Sasaki, H., 2008. Precise remote-monitoring technique of water volume and temperature of a crater lake in Aso volcano, Japan: implications for a sensitive window of a volcanic hydrothermal system. *Earth Planets Space* 60, 705–710.
- Tsunematsu, K., Ishimine, Y., Kaneko, T., Yoshimoto, M., Fujii, T., 2016. Estimation of ballistic block landing energy during 2014 Mount Ontake eruption. *Earth Planets Space* 68, 88.
- Walker, G.P.L., 1971. Grain-size characteristics of pyroclastic deposits. *J. Geol.* 79, 696-714.
- Walker, G.P.L., 1983. Ignimbrite types and ignimbrite problems. *J. Volcanol. Geotherm. Res.* 17, 65-88.
- Yokoo, A., Miyabuchi, Y., 2015. Eruption at the Nakadake 1st crater of Aso Volcano started in November 2014. *Bull. Volcanol. Soc. Japan* 60, 275-278 (in Japanese).

## Figure captions

**Table 1** Major element compositions of glass shards included in the September 14, 2015, May 2015, November 2014, April 20, 1990 and September 6, 1979 eruption deposits from Nakadake first crater.

**Fig. 1.** (A) Distribution map of the September 14, 2015 ash-fall deposit from Nakadake first crater. Dotted line shows the extent of the September 14 pyroclastic density currents (PDCs). (B) Distribution of the September 14 PDC deposits around Nakadake crater. 1st, 2nd, 3rd and 4th-7th indicate the Nakadake first crater (eruption vent), second crater, third crater and fourth-seventh craters, respectively. (C) Photograph of the September 14, 2015, eruption of Nakadake first crater taken at a site 3 km west of the crater (locality A in Fig. 1A) (photo credit: Yuka Matsushima).

**Fig. 2.** (A) Numerous ballistic clasts scattered at the southern rim of the Nakadake second crater (locality G in Fig. 1B). Poles of woody fence are ca. 1 m in height. (B) Woody fence destroyed by impacts of ballistics at the southern crater rim (loc. H). (C) Numerous ballistic clasts scattered at the southwestern rim of the Nakadake first crater (loc. I). (D) Largest ballistic rock produced by the September 14 eruption (loc. K). Scale segments are 10 cm. These photos were taken in the morning of September 15, 2015.

**Fig. 3.** (A) Ballistic clasts deposited in an area of  $2.2 \times 1.7$  m (ca.  $3.5$  m<sup>2</sup>) on the roof

top of a camera cabin of the Aso Volcano Museum located at the southwestern rim of Nakadake first crater (locality J in Fig. 1B). (B) Representative examples of ballistic clasts ejected by the September 14 eruption.

**Fig. 4.** Size, mass, bulk volume and density of ballistic clasts ejected by the September 14, 2015 eruption.

**Fig. 5.** Weight inside an ash sampler installed at the southwestern rim of the Nakadake first crater (loc. J in Fig. 1B). (A) The upside of the weight. (B) The underside of the weight which was partially melted by heat of a ballistic clast.

**Fig. 6.** Aerial photo showing the extent of pyroclastic density currents from Nakadake first crater. The photograph was taken from the southeast by the Japan Meteorological Agency with Kyushu Regional Development Bureau (Ministry of Land, Infrastructure, Transport and Tourism) in the afternoon of September 14, 2015.

**Fig. 7.** Proximal September 14, 2015 eruption deposits at 0.3 km SW of the center of Nakadake first crater (loc. L in Fig. 1B). Scale in centimeters. The photo was taken in the morning of September 15, 2015.

**Fig. 8.** September 14 ash-fall deposit about 2.8 km WNW (A; locality B in Fig. 1A) and 1.7 km NW (B; loc. C) of the Nakadake first crater. The photos were taken on September 14, 2015.

**Fig. 9.** (A) Grain-size histograms coarser than 5  $\phi$  (1/32 mm) of representative samples from the September 14, 2015 eruption deposits. Proportions of components coarser

than 3  $\phi$  of only four samples are shown. (B) Proportions of components for fraction 2-3  $\phi$  of the September 14 Nakadake eruption deposits. Data of the September 6, 1979 and April 20, 1990 ash are presented for comparison. (C) Proportions of glass types included in the September 14 Nakadake eruption deposits (fraction of 2-3  $\phi$ ).

**Fig. 10.** (A) Plot of median diameter ( $Md_{\phi}$ ) versus sorting coefficient ( $\sigma_{\phi}$ ) of grain-size data (finer than -5  $\phi$  fraction) for the September 14, 2015 Nakadake eruption deposits; Unzen 1991-1995 block-and-ash flow, ash-cloud surge and ash-fall deposits (Miyabuchi, 1999); Nakadake 19 ka bomb-and-ash flow deposit (Miyabuchi et al., 2006). (B) Plots of weight percentage of particles finer than 1/16 mm (F2) versus weight percentage of particles finer than 1 mm (F1). The outlined areas represent the 1% contour fields of Walker (1971, 1983) for pyroclastic-flow and -surge deposits.

**Fig. 11.** Polarizing microscope photographs of the September 14, 2015 ash and ballistic clasts. (A) Particles included in the ash-fall deposit at 1.7 km NW of Nakadake first crater (location C in Fig. 1A). BkG: black glass, BrG: brown glass, C: crystal, L: lithic, PBG: pale brown glass. (B) Fresh ballistic clast. (C) Weakly altered clast. (D) Highly altered ballistic clast.

**Fig. 12.** Secondary electron micrographs of typical glass shards included in the September 14 ash-fall deposit (A, B) and pyroclastic density current deposit (C, D) from the Nakadake first crater.

**Fig. 13.** Major element compositions in wt% of glass shards included in the September 14 eruption deposits. Analytical values of the May 2015, November 2014, April 20, 1990 and September 6, 1979 ashes from Nakadake first crater are also plotted for comparison.

**Fig. 14.** Back-scattered electron micrographs of representative glass shards included in the September 14 deposits. (A) Pale brown and black glass shards in the upper part of September 14 PDC deposit (unit 2). (B) Pale brown glasses in September 14 ash-fall deposit (unit 3). (C) and (D) Black glasses in the lower part of PDC deposit (unit 1). (E) Black glass shard (the upper part of PDC deposit) including numerous nanolites. (F) Microlites (>1  $\mu\text{m}$ ) and nanolites contained in a glass grain of the September 14 ash-fall deposit.

**Fig. 15.** X-ray diffraction (XRD) patterns of September 14, 2015, April 20, 1990 and September 6, 1979 ash-fall deposits. Abbreviations for minerals: Al: alunite, J: jarosite, M: montmorillonite, Q: quartz, Z: zeolite.

**Fig. 16.** Schematic reconstruction of September 14, 2015 eruption sequence at the Nakadake first crater.

**Table 1**

Major element compositions of glass shards included in the September 14, 2015, May 2015, November 2014, April 20, 1990 and September 6, 1979 eruption deposits from Nakadake first crater.

| Eruption date<br>Sample name   | Sept 14 2015  |      |   |      | May 2015 (ash eruption deposits)                         |      |  |      | Nov 2014 (ash eruption deposits)   |      |                                |      |                                 |      | Apr 20 1990                         |      | Sept 6 1979                         |      |                                 |      |                                 |      |
|--------------------------------|---|------|---|------|--|------|--|------|------------------------------------|------|--------------------------------|------|---------------------------------|------|-------------------------------------|------|-------------------------------------|------|---------------------------------|------|---------------------------------|------|
|                                | Sept 14 2015 PDC<br>deposit (pale brown<br>glasses) |      | Sept 14 2015 PDC<br>deposit (black to<br>brown glasses) |      | Sept 14 2015 ash-fall<br>deposit (pale brown<br>glasses) |      | Sept 14 2015 ash-fall<br>deposit (black to<br>brown glasses) |      | May 4-11 2015 ash-<br>fall deposit |      | May 3 2015 ash-fall<br>deposit |      | Nov 25 2014 ash-fall<br>deposit |      | Nov 25-27 2014 ash-<br>fall deposit |      | Nov 27-29 2014 ash-<br>fall deposit |      | Apr 20 1990 ash-fall<br>deposit |      | Sept 6 1979 ash-fall<br>deposit |      |
|                                | AV (wt.%)   | STD  | AV (wt.%)   | STD  | AV (wt.%)  | STD  | AV (wt.%)  | STD  | AV (wt.%)                          | STD  | AV (wt.%)                      | STD  | AV (wt.%)                       | STD  | AV (wt.%)                           | STD  | AV (wt.%)                           | STD  | AV (wt.%)                       | STD  | AV (wt.%)                       | STD  |
| SiO <sub>2</sub>               | 58.15   | 0.72 | 58.40   | 1.02 | 57.98  | 1.08 | 58.36  | 1.13 | 57.42                              | 0.94 | 57.43                          | 1.16 | 58.88                           | 1.32 | 58.50                               | 1.36 | 58.70                               | 1.14 | 57.16                           | 0.72 | 57.44                           | 0.84 |
| TiO <sub>2</sub>               | 1.41  | 0.10 | 1.43  | 0.16 | 1.33   | 0.13 | 1.37   | 0.11 | 1.33                               | 0.13 | 1.33                           | 0.15 | 1.30                            | 0.25 | 1.35                                | 0.21 | 1.43                                | 0.24 | 1.32                            | 0.11 | 1.36                            | 0.11 |
| Al <sub>2</sub> O <sub>3</sub> | 14.02   | 0.26 | 14.08   | 0.27 | 14.00  | 0.29 | 14.16  | 0.30 | 14.41                              | 0.42 | 14.29                          | 0.85 | 14.96                           | 1.08 | 14.02                               | 0.87 | 14.05                               | 1.19 | 14.45                           | 0.26 | 14.58                           | 0.46 |
| FeO*                           | 9.84  | 0.37 | 10.01   | 0.77 | 9.89   | 0.42 | 9.80   | 0.64 | 9.53                               | 0.87 | 9.62                           | 1.05 | 9.37                            | 1.59 | 9.64                                | 1.09 | 9.49                                | 1.51 | 9.63                            | 0.40 | 9.51                            | 0.49 |
| MnO                            | 0.15  | 0.08 | 0.17  | 0.10 | 0.16   | 0.08 | 0.14   | 0.08 | 0.13                               | 0.05 | 0.16                           | 0.04 | 0.14                            | 0.05 | 0.18                                | 0.04 | 0.17                                | 0.05 | 0.18                            | 0.07 | 0.20                            | 0.07 |
| MgO                            | 2.80  | 0.16 | 2.87  | 0.33 | 2.81   | 0.22 | 2.75   | 0.46 | 2.65                               | 0.42 | 2.76                           | 0.42 | 2.52                            | 0.85 | 2.62                                | 0.56 | 2.67                                | 0.58 | 2.90                            | 0.22 | 2.90                            | 0.46 |
| CaO                            | 6.30  | 0.22 | 6.25  | 0.44 | 6.35   | 0.35 | 6.56   | 0.87 | 5.85                               | 0.45 | 5.91                           | 0.63 | 5.93                            | 1.16 | 5.65                                | 0.84 | 5.67                                | 0.84 | 6.17                            | 0.34 | 6.04                            | 0.58 |
| Na <sub>2</sub> O              | 2.87  | 0.39 | 2.55  | 0.44 | 3.00   | 0.26 | 2.54   | 0.78 | 2.66                               | 0.56 | 2.52                           | 0.63 | 3.21                            | 0.48 | 2.93                                | 0.35 | 2.71                                | 0.45 | 2.76                            | 0.38 | 2.40                            | 0.71 |
| K <sub>2</sub> O               | 3.20  | 0.26 | 3.44  | 0.40 | 3.29   | 0.20 | 2.80   | 0.51 | 3.09                               | 0.52 | 3.06                           | 0.55 | 3.22                            | 0.57 | 3.35                                | 0.63 | 3.26                                | 0.57 | 3.05                            | 0.15 | 2.81                            | 0.53 |
| Total                          | 98.74   | 0.89 | 99.19   | 0.83 | 98.80  | 0.99 | 98.49  | 0.77 | 97.07                              | 0.64 | 97.09                          | 0.65 | 99.53                           | 0.80 | 98.24                               | 0.99 | 98.17                               | 1.42 | 98.14                           | 0.86 | 97.80                           | 0.89 |
| N                              | 53  |      | 15  |      | 47   |      | 22   |      | 35                                 |      | 89                             |      | 58                              |      | 29                                  |      | 28                                  |      | 145                             |      | 79                              |      |

Analyses presented as a mean (AV) and standard deviation (STD). FeO\*, total iron oxide as FeO; N, number of analyses.





Figure 2

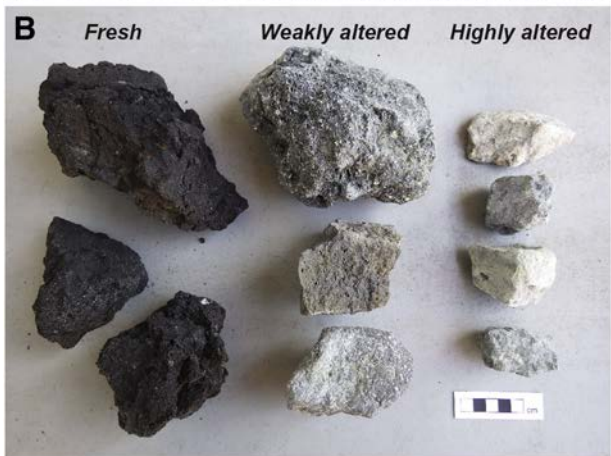
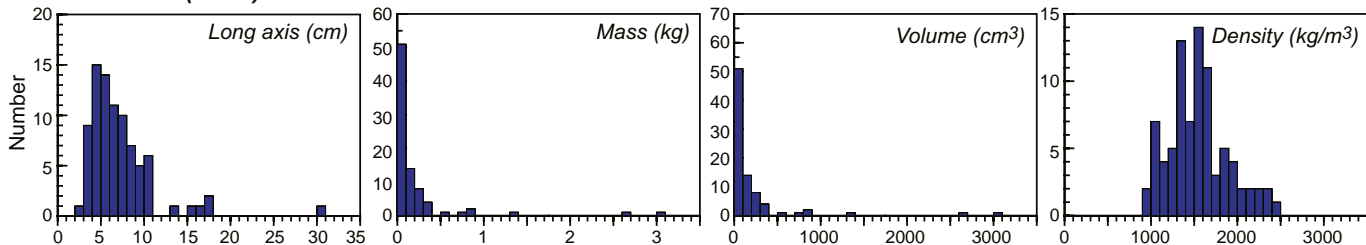


Figure 3

### Fresh clasts (N=84)



### Weakly altered clasts (N=42) and Highly altered clasts (N=32)

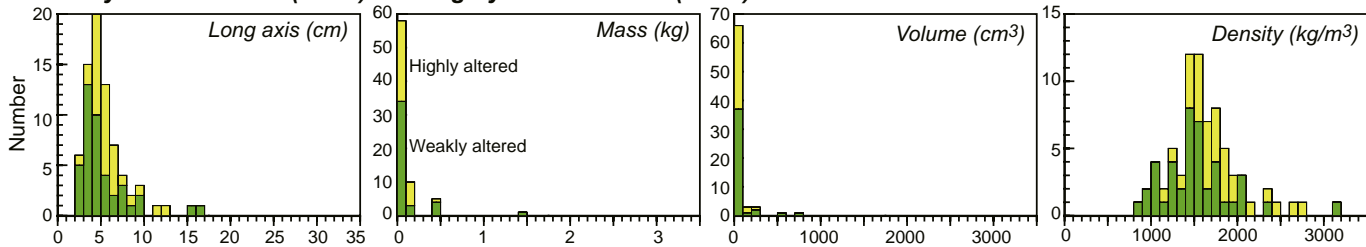


Figure 4



Figure 5



Figure 6

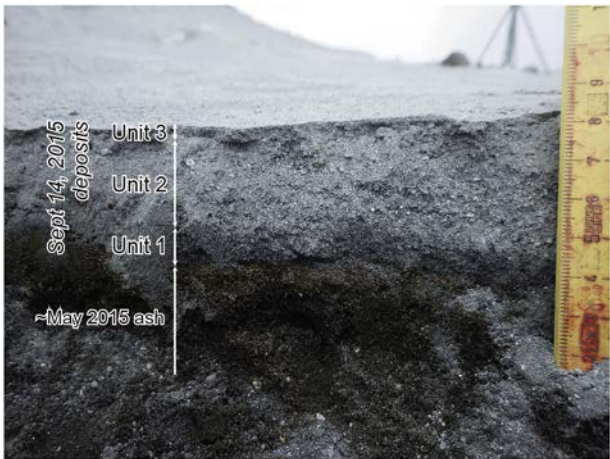


Figure 7

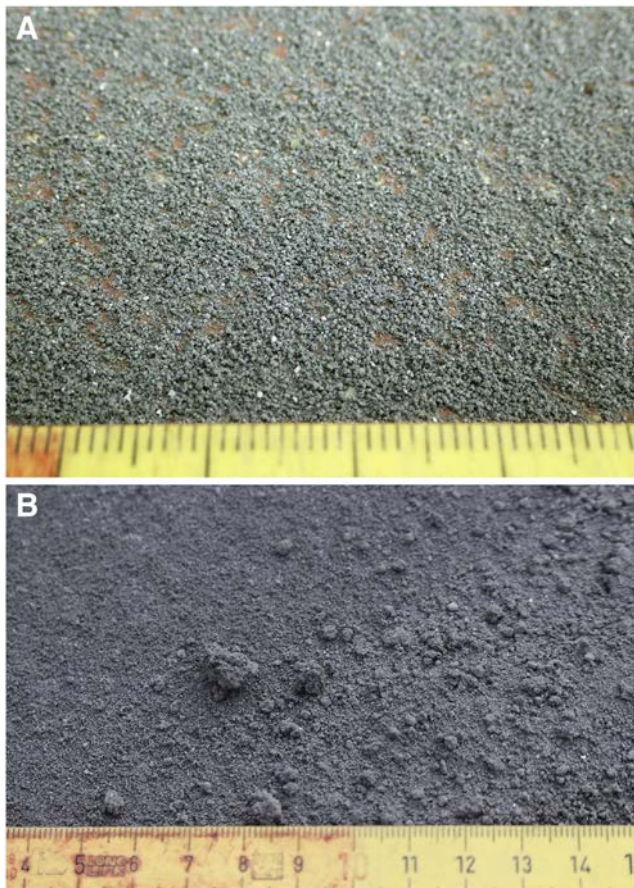
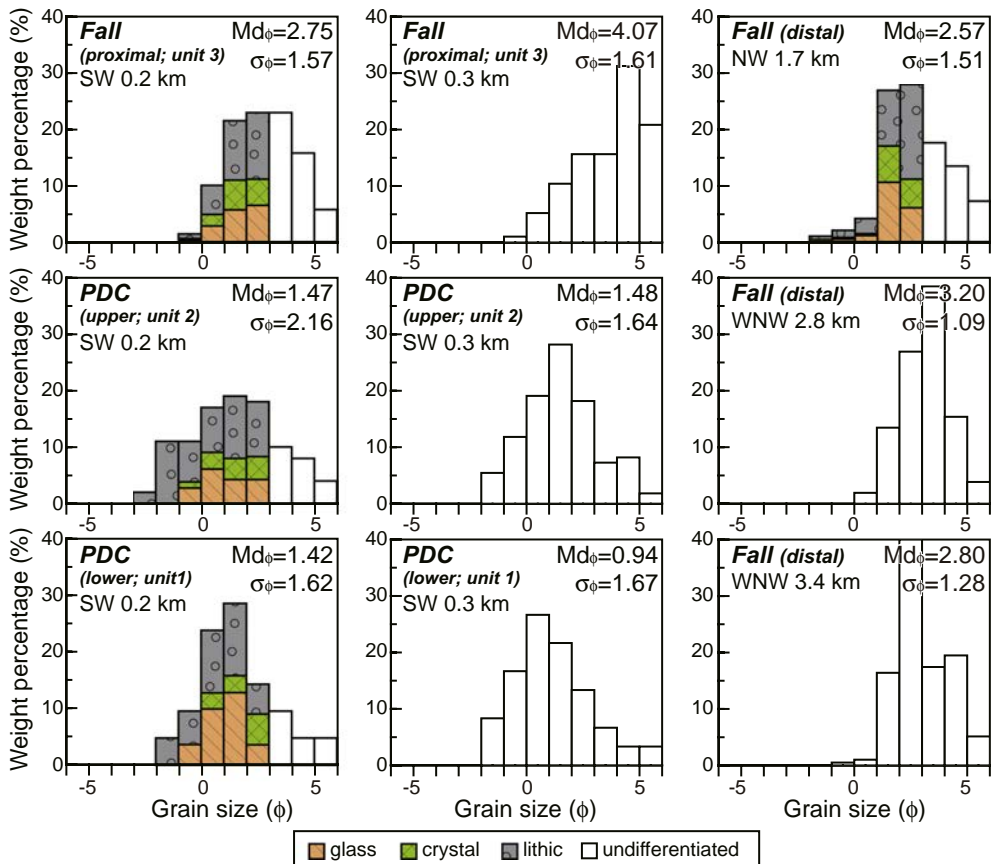
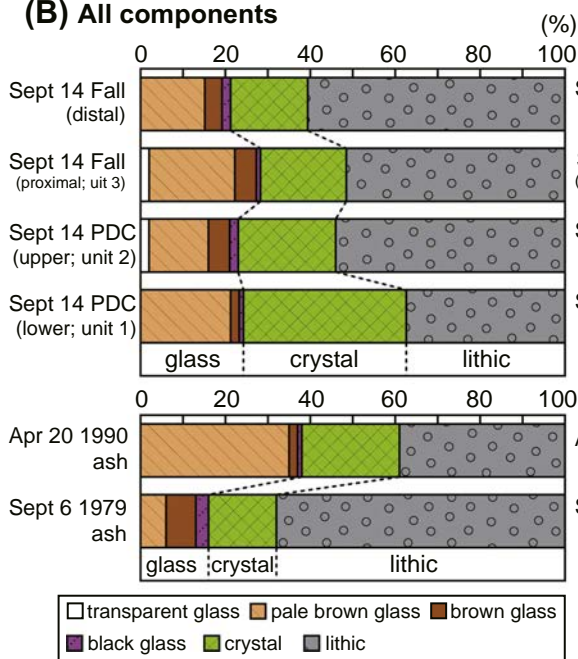


Figure 8

### (A) Grain-size histograms



### (B) All components



### (C) Glass morphology type

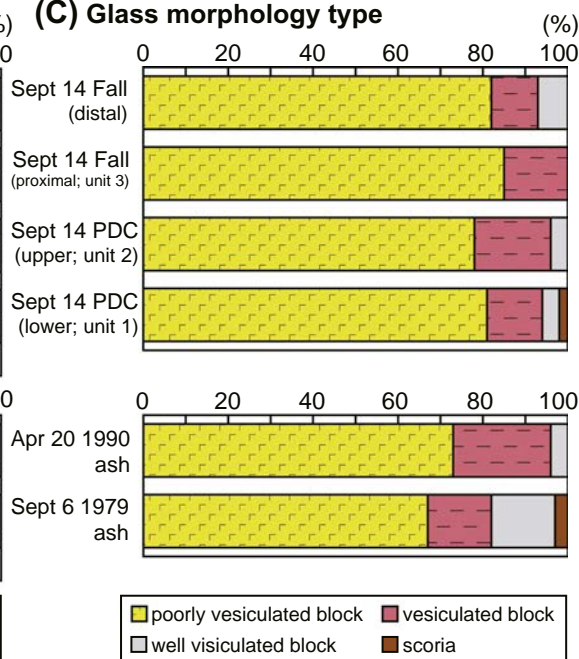


Figure 9

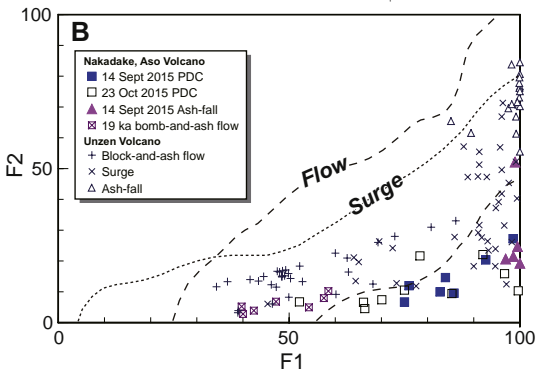
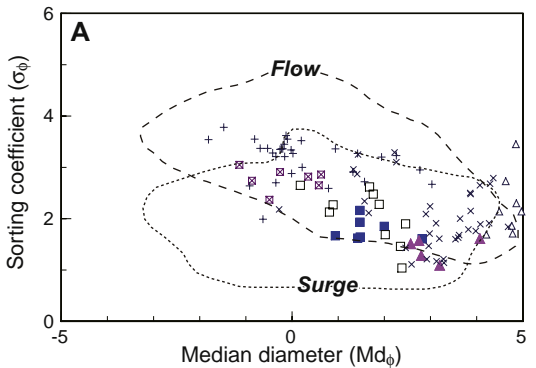


Figure 10



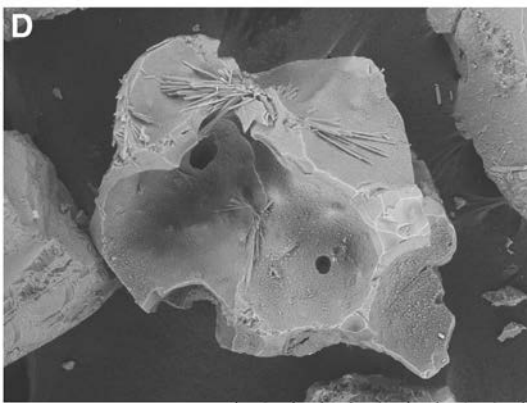
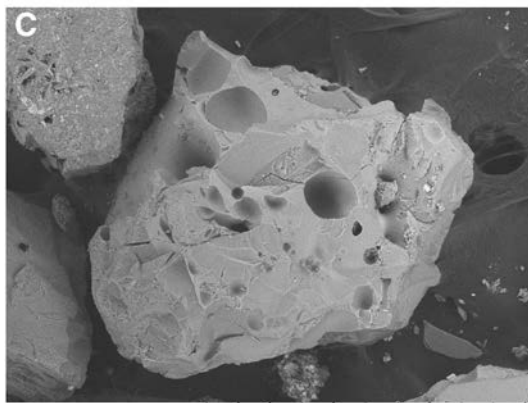
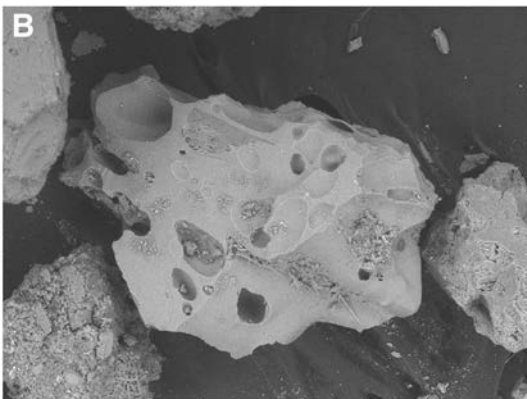
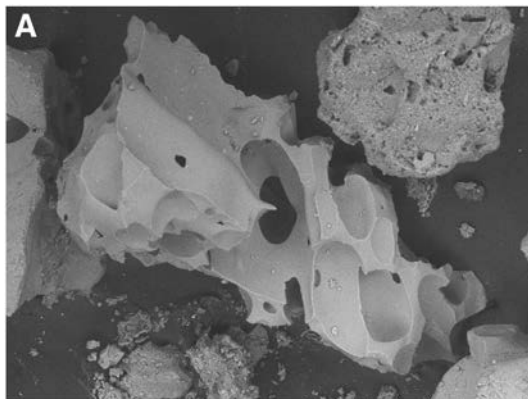


Figure 12

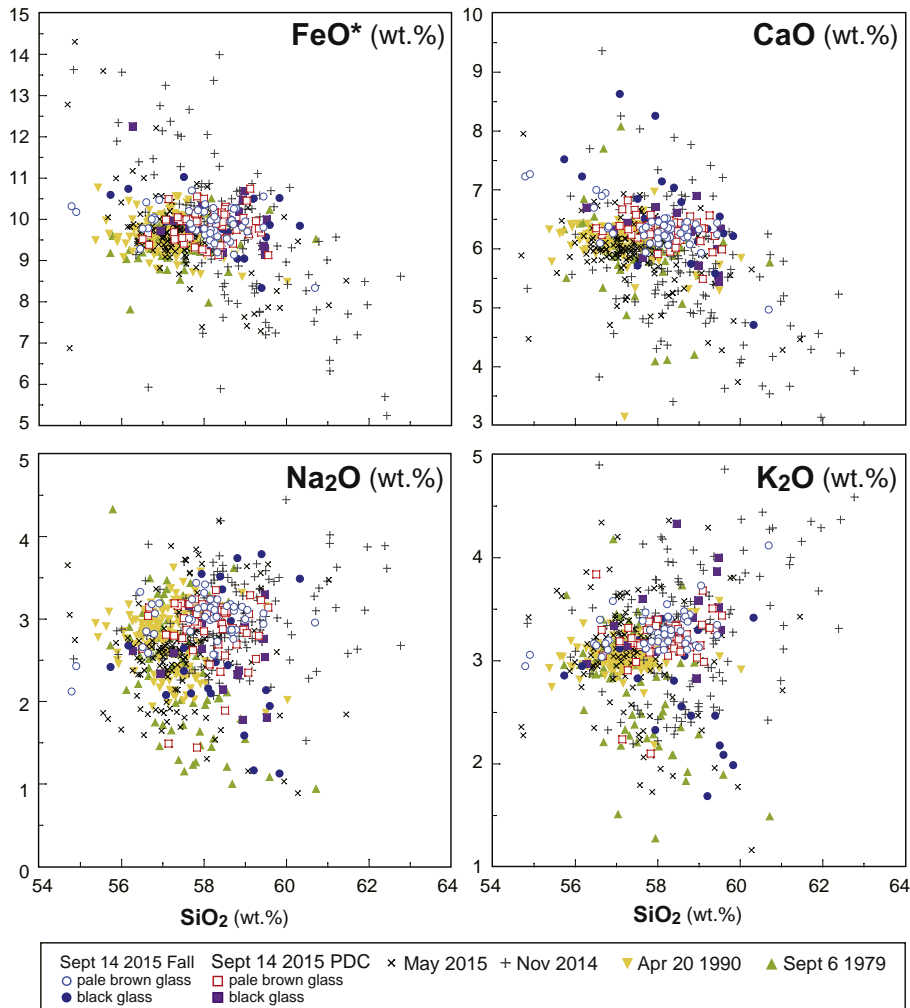


Figure 13

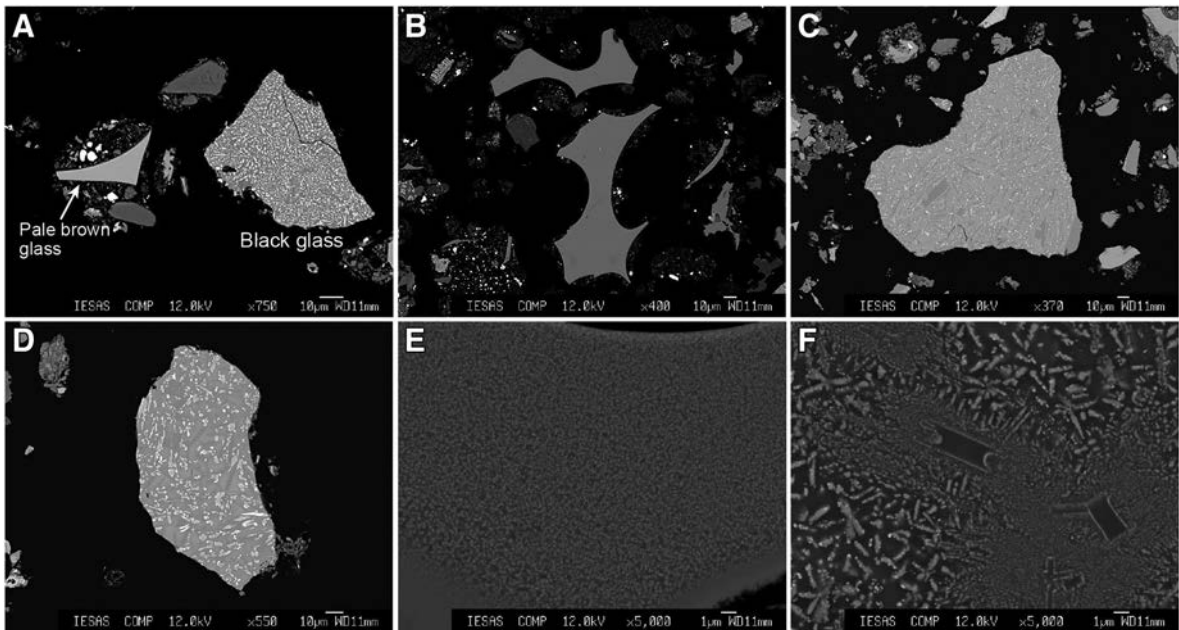


Figure 14

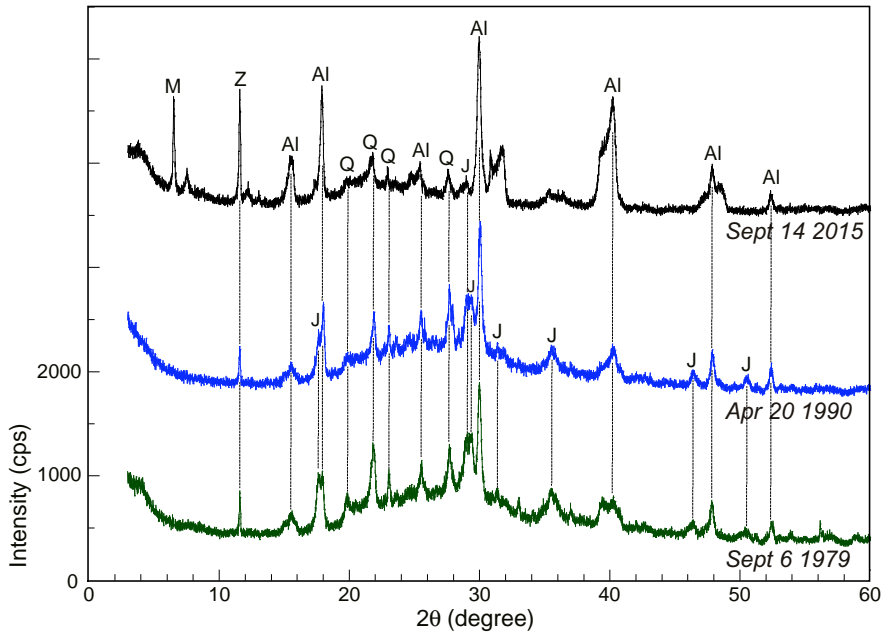
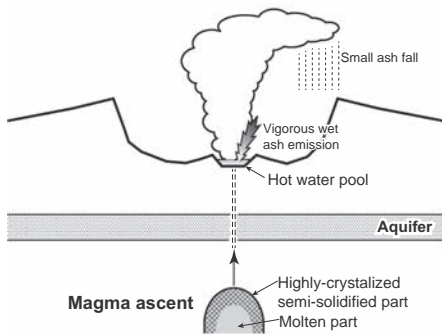


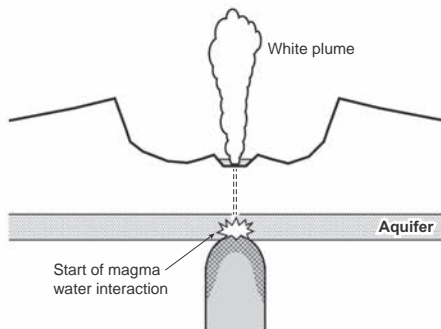
Figure 15

**(A) 4 days before**

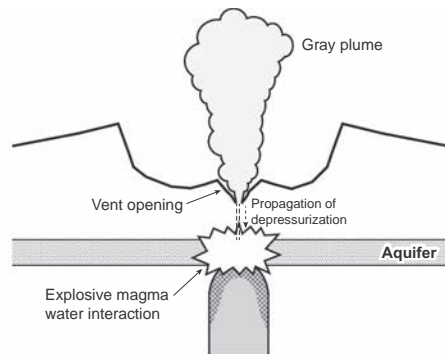
(Sept 10~)



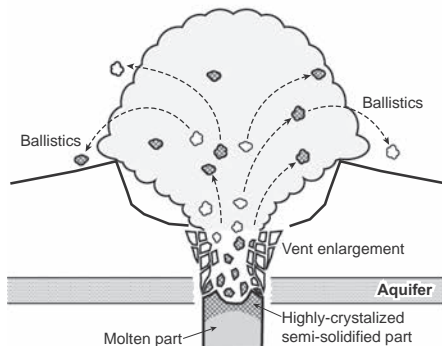
**(B) Sept 14 09:18~**



**(C) Sept 14 09:43~**



**(D) Sept 14 09:47:07~**



**(E) Sept 14 09:47:14-09:48:30**

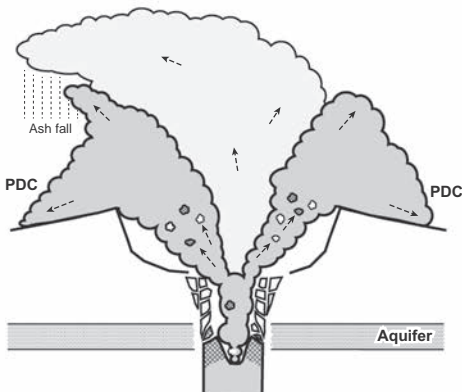


Figure 16